Eur. Phys. J. D **38**, 59–64 (2006)
DOI: 10.1140/epjd/e2005-00327-x

THE EUROPEAN PHYSICAL JOURNAL D

Angular dependence of double electron capture in collisions of C^{4+} with He

Stueckelberg oscillations in the differential cross-section for capture into $C^{2+}(1s^2 2s^2\ ^1S)$

L. Pichl[1,a], R. Suzuki[2], M. Kimura[3], Y. Li[4], R.J. Buenker[4], M. Hoshino[5], and Y. Yamazaki[6]

[1] Max Planck Institute for the Physics of Complex Systems, Nöthnitzer Str. 38, 01187 Dresden, Germany
[2] Computer Center, Hitotsubashi University, Kunitachi, Tokyo 186-8601, Japan
[3] Graduate School of Sciences, Kyushu University, Fukuoka 812-8581, Japan
[4] Fachbereich C-Mathematik und Naturwissenschaften, Bergische Universität Wuppertal, 42119 Wuppertal, Germany
[5] Department of Physics, Sophia University, 7-1 Kioicho, Tokyo 102-8554, Japan
[6] RIKEN, 2-1 Hirosawa, Wako 351-0198, Japan

Received 2 August 2005 / Received in final form 28 October 2005
Published online 13 December 2005 –

Abstract. In charge-transfer collisions of $C^{4+}(1s^2\ ^1S)$ with He $(1s^2\ ^1S)$, the process of double electron capture into the ground state C^{2+} is well-known to dominate other channels by an order of magnitude for projectile energies below 10 keV. This work presents a calculation of differential cross-sections resolved in the angle and energy gain variables, based on an ab initio treatment of electronic states, and compares with the measurements published in the literature (projectile energy $E = 270$, 400, and 470 eV). We also briefly discuss the semi-empirical two-state models developed by experimentalists for this process.

PACS. 34.70.+e Charge transfer – 31.15.Ar Ab initio calculations

1 Introduction

Experimental data on electron capture in charge transfer collisions of C^{4+} with He have been abundant in the literature, both for integral and angle-differential cross-sections [1–5]. By contrast, theoretical works based on ab initio potentials are extremely scarce; this is in part due to the difficulty in calculating the interaction between the closed $1s^2$ shells of C^{4+} ion and He atom. The most elaborate theoretical work to date presents a calculation of integral single-capture (SC) and double-capture (DC) cross-sections by Kimura and Olson [6], who used an ion-core pseudo-potential for $C^{2+}(1s^2)$, dealing explicitly with the two active valence electrons. Reference [6] provides the integral cross-section data for projectile energies between 750 eV and 200 keV.

To date, experimentalists have mostly relied upon semi-empirical representations of the system (e.g. 2-state model in Ref. [3] or 4-state model in Ref. [4]), using polarization and Coulomb-type diabatic potentials with position-dependent effective charges, or potentials defined as an interpolation between the asymptotic terms for low and large internuclear distance R. In either case, the coupling between the diabatic states was estimated by an elaborate analytical formula of Grozdanov and Janev [7] with adjusted parameters. Model potential curves were also used to deduce the diabatic coupling in an inverse problem (fitting model to cross-section data) [8], resulting in different coupling terms than in reference [7]. By using free parameters in the model formulas, experimental data could be modelled rather accurately, yet the potentials and coupling terms vary among the experimental groups. Clearly, since CHe^{4+} is now an inexpensive 4-electron system even for large basis sets, a full ab initio calculation is therefore preferable. The differential cross-sections also depend more strongly on the details of the interaction, and represent a stricter test on the accuracy of theory as compared to the integral cross-sections published before [6].

Here we calculate the differential cross-sections for the above process, motivated by recent publications of state-resolved angle-differential and energy-gain differential cross-sections in the literature [1,2]. The differential cross-sections for the main capture channel are evaluated in both equivalent forms, and compared with the experimental data available for the collision energy $E = 270$, 400 and 470 eV.

The paper is organized as follows. Section 2 summarizes the ab initio calculation and compares the resulting potentials and couplings to empirical models used by experimentalists. Section 3 briefly explains the standard

[a] e-mail: lukas@pichl.jp
On summer leave from: International Christian University, Osawa 3-10-2, Mitaka, Tokyo 181-8585, Japan.

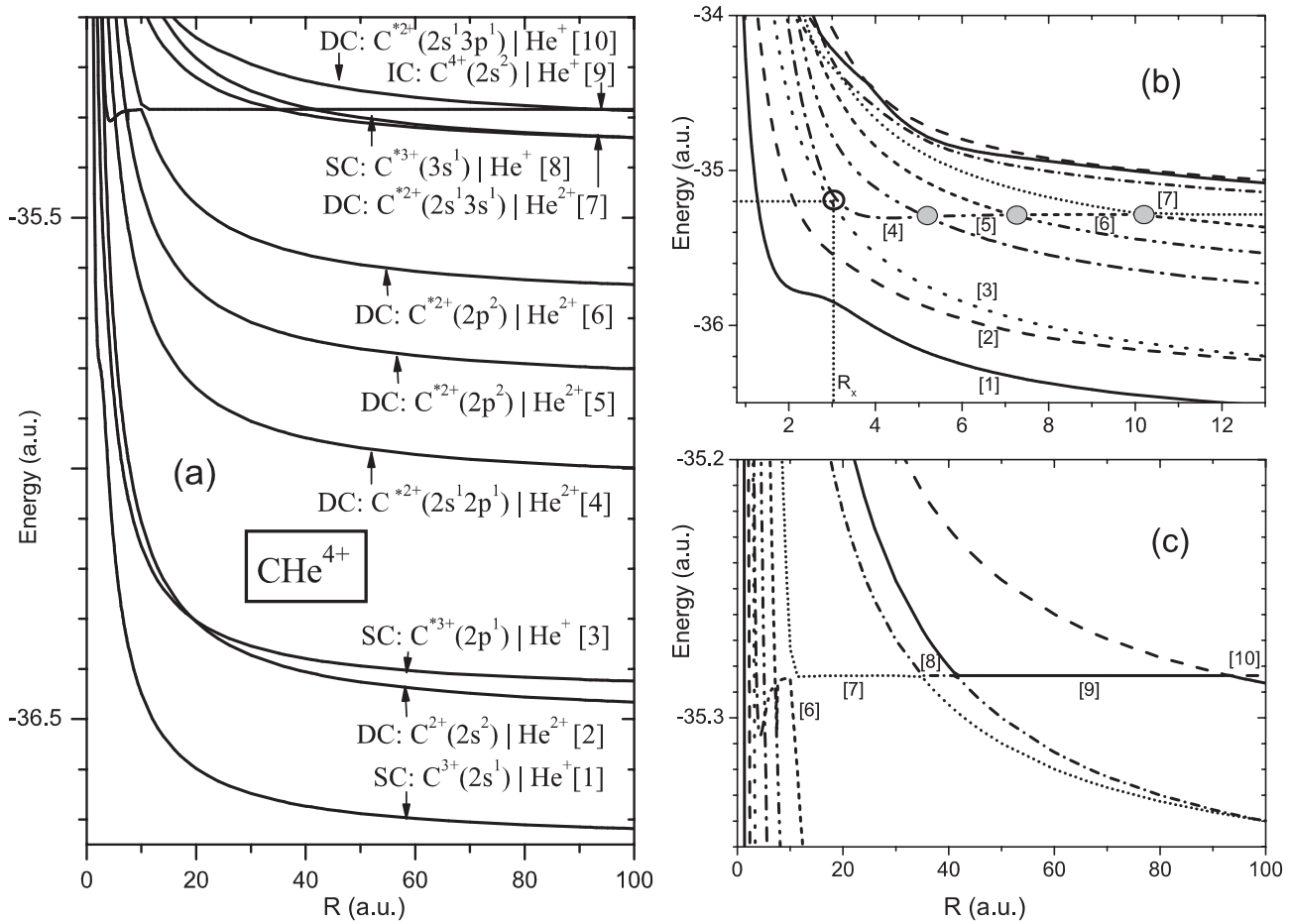

Fig. 1. Potential energy curves of CHe^{4+}: (a) overall behavior and asymptotic assignments of the initial channel (IC), single electron capture channels (SC) and double electron capture channels (DC); (b) transition region and location of the crossing point R_x; (c) detailed view of the potential energy curves. The horizontal line (consisting of several adiabatic state components) corresponds to the initial state $C^{4+}(1s^2\ ^1S)|He(1s^2\ ^1S)$. All other curves show Coulomb potential asymptotics (SC and DC states).

theoretical procedure and lists the kinematic and cross-section transform relations in order to compare with experiment. Results are discussed in Section 4. Section 5 concludes the paper. Atomic units are used throughout unless mentioned otherwise.

2 Electronic states of CHe^{4+}

In order to obtain the potential curves of the C^{4+}/He system, we have carried out ab initio configuration interaction calculations by using an extended version of the multireference single- and double-excitation MRD-CI programs [9]. The correlation consistent polarized valence quadruple zeta, cc-pVQZ Gaussian basis [10] was employed for the C and He atoms. A selection threshold of 10^{-9} Hartree was used to select the configuration wave functions of which the electronic wave functions are composed. Potential energy curves for nine low-energy charge-transfer states significantly coupled to the initial channel were computed for R between 0.8 and 110. Corresponding nonadiabatic couplings $\langle Q(R)_i|\mathrm{d}Q(R)_j/\mathrm{d}R\rangle$ were evaluated by using a numerical differentiation method.

Figure 1 shows the resulting manifold of potential energy curves for the electronic states considered in the calculation. In Figure 1a, the potential energy curves are labeled with the asymptotic assignment of the respective states, which corresponds either to the initial channel ($C^{4+}|He$), single-capture ($C^{3+}|He^{+}$) or double capture ($C^{2+}|He^{2+}$) states. In addition, adiabatic states are numbered with increasing energy in Figure 1a. The location of the avoided crossing point at $R = R_x$, which mediates the double electron capture, is shown in Figure 1b. This crossing point between states No. 3 and 4 at R_x is denoted by an empty circle in Figure 1b. Note also the sequence of diabatic curve crossings between states 4-5, 5-6, and 6-7 therein (grey circles). This sequence of crossings is further continued in Figure 1c up to the asymptotic region along the horizontal line, which corresponds to the $1s^2 - 1s^2$ electronic configuration of initial state. Except for the crossing point at R_x, the behavior of all other avoided crossing is dominantly diabatic, i.e. the minimal

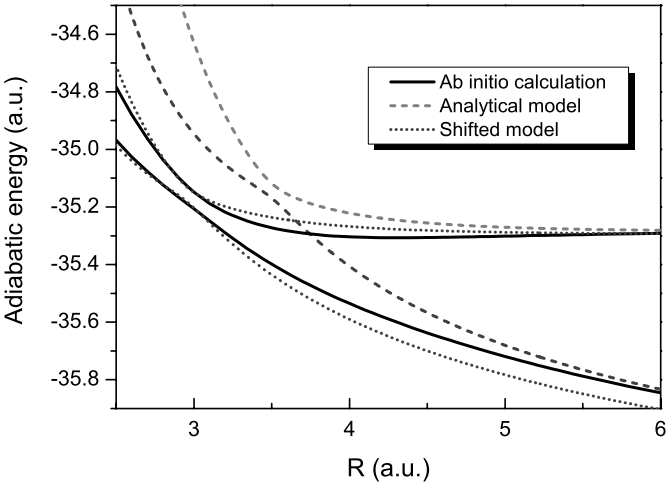

Fig. 2. Adiabatic curves: two-state model.

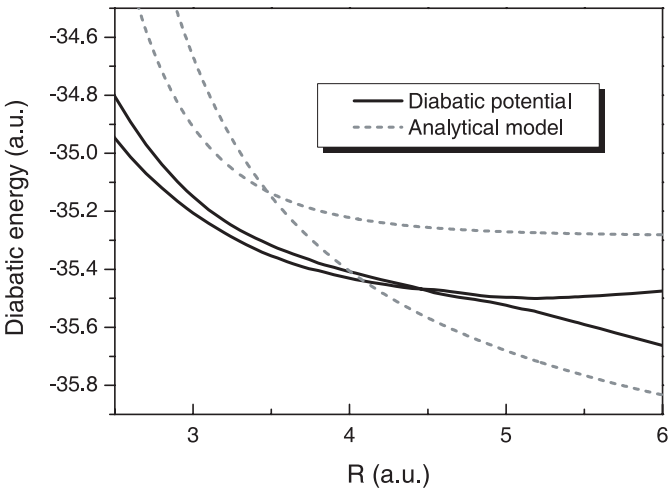

Fig. 3. Diabatic curves: two-state model.

separation of adiabatic curves is very small, major electronic configurations of each crossing pair of the adiabatic states are mutually exchanged at either side of the crossing point, and the corresponding derivative coupling term exhibits a narrow peak at each diabatic crossing. The potential energy in the initial collision state remains flat over a long region of distance, because the first interaction correction, the polarization term between C^{4+} and He, behaves as $\sim R^{-4}$. The potential in the electron capture channels decays as $3/R$ (SC) or $4/R$ (DC) at large values of R. All capture processes are driven by the behavior of electronic states and their nonadiabatic coupling (both radial and angular components) at shorter distances, where exothermic transitions may take place.

The avoided crossing in Figure 1b ($R_x \sim 3$) is by large the main transition mechanism for the double electron capture, which can be seen from the behavior of potential energy curves 3 and 4 in the vicinity of the crossing point, and is also supported by the analysis of corresponding nonadiabatic couplings. At the transition region, the FWHM of the broad coupling peak is $R_{FWHM} \sim 0.38$ a.u., and throughout this region the two potential energy curves are almost parallel. It is well known that nonadiabatic transitions easily occur at avoided crossings of this type [11].

The crossing point features can be seen in Figure 2 in more detail, along with the empirical potential curves used by Danared and Barany in analytical form [3] (dashed line). The crossing point calculated here is 0.5 a.u. lower than that of the model potentials (dashed line) [3]. The adiabatic curves from our calculation coincide well with the model potentials shifted to the transition point (dotted line) throughout the entire transition region, but differ at larger distances. Such a difference should not have an impact on the transition probabilities, although it may appear as a phase in the scattering amplitudes.

Figure 3 shows the diabatic potentials, which are obtained by a rotation matrix $\underline{C}$ applied on the 2-by-2 diagonal matrix of adiabatic potentials. The matrix $\underline{C}$ satisfies

$$\underline{C}(R) = \underline{I} + \int_R^\infty \underline{A}(R')\underline{C}(R')\mathrm{d}R', \qquad (1)$$

where $A_{i,j}(R) = (1-\delta_{i,1-j})\langle i|\mathrm{d}/\mathrm{d}R|j\rangle$ for $i,j = 1,2$. In the basis of electronic states rotated by $\underline{C}(R)$, all nonadiabatic coupling terms identically vanish. Such a representation is required in the full quantum calculations [12,13]. The present results differ significantly from those based on the shifted diabatic potentials. This is plausible since in general, the adiabatic potential matrix includes only the two eigenvalues, while a full 2-by-2 Hamiltonian matrix consists of three independent elements, and in particular it depends on the behavior of the derivative coupling term.

3 Charge transfer collision dynamics

In this section, we review the standard kinematic relations and reference frame transforms [14], and summarize the procedure to obtain differential cross-sections.

The angle-differential cross-section in the laboratory system (angle θ_L) consists of two contributions in the center-of-mass frame,

$$\theta_{CMS\pm} = \cos^{-1}\left[-\xi\sin^2\theta_L \pm (1-\xi^2\sin^2\theta_L)^{1/2}\cos\theta_L\right], \qquad (2)$$

with $\xi = m_1 v_i/(m_2 v_f)$, where $m_{1,2}$ is the mass of the projectile and the target, respectively, and $v_{i,f}$ the initial and final relative velocity. The differential cross-sections then transform as

$$\frac{\mathrm{d}\sigma}{\mathrm{d}\Omega_L}(\theta_L) = \frac{\left(1+2\xi\cos\theta_L+\xi^2\right)^{3/2}}{|1+\xi\cos\theta_L|}\frac{\mathrm{d}\sigma}{\mathrm{d}\Omega_{CMS}}(\theta_{CMS}), \qquad (3)$$

for scattering angles up to the maximum $\theta_{L,max} = \sin^{-1}\xi^{-1}$.

Given a particular gain/loss of projectile internal energy Q in the scattering event, the energy gain of the projectile (energy E_0) and the scattering angle are equivalent,

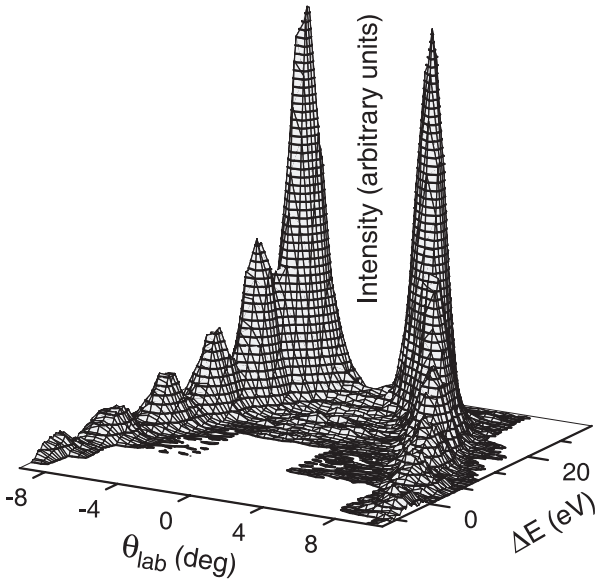

Fig. 4. Double-differential cross-section for double electron capture to $C^{2+}(1s^2 2s^2\ ^1S)$.

according to

$$\Delta(E) = \left(\frac{m_1}{m_1+m_2}\right)^2 E_0 \cos^2\theta_L \times \left\{1+\left[1-\frac{m_2^2+m_1 m_2}{m_1^2\cos^2\theta_L}\left(\frac{m_1}{m_2}-1-\frac{Q}{E_0}\right)\right]^{1/2}\right\}^2 - E_0, \quad (4)$$

which yields the cross-section transform

$$-\frac{\mathrm{d}\sigma}{\mathrm{d}(\Delta E)} = \frac{\pi(m_1+m_2)^2(1+\gamma/\cos^2\theta_L)^{1/2}}{m_1^2 E_0 \cos\theta_L[1+(1+\gamma/cos^2\theta_L)^{1/2}]^2}\frac{\mathrm{d}\sigma}{\mathrm{d}\Omega_L(\theta_L)}. \quad (5)$$

The de Broglie wave length of the projectile at the lowest energy considered in this work is 1.5×10^{-3} a.u., due to the large mass of the C^{4+} projectile, and much below the characteristic distance of the potential matrix. Therefore we apply the eikonal approximation for solving the coupled equations for state-dependent amplitudes $c_{j,i_0}(b,z)$, $j = 1, 10$. The semiclassical formulation of these equations is given in detail in references [15,16] (cf. also references therein) and thus will not be repeated here. The cross-section then follows from the diffraction integral,

$$\frac{\mathrm{d}\sigma}{\mathrm{d}\Omega}(\theta) = (mv)^2 \left| \int_0^\infty J_0(\eta b) c_{f i_0}(b;\infty) b \mathrm{d}b \right|^2, \quad (6)$$

where m is the reduced mass, v is the relative collision velocity, J_0 is the Bessel function and $\eta = 2mv\sin(\theta/2)$ [15]. To calculate the diffraction integral in equation (6), we employ a 10,000-point grid of impact parameters.

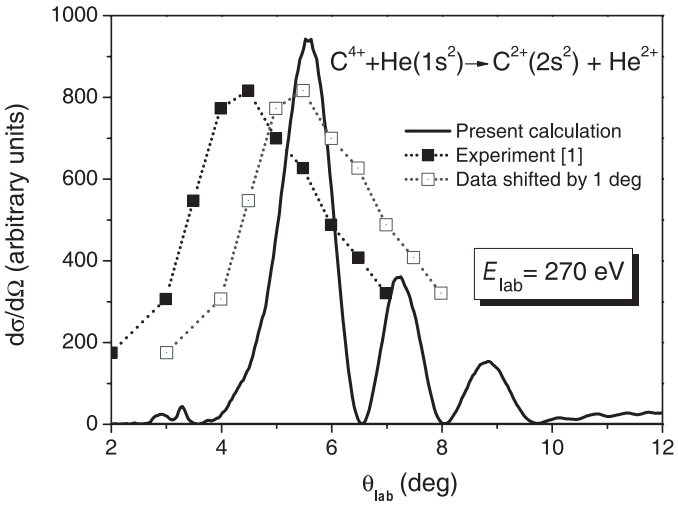

Fig. 5. Angle-differential cross-section for electron double capture to $C^{2+}(1s^2 2s^2\ ^1S)$ at 270 eV.

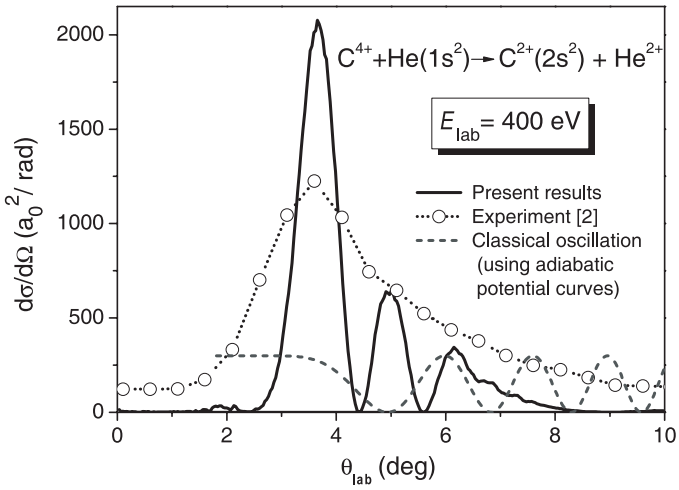

Fig. 6. Angle-differential cross-section for electron double capture to $C^{2+}(1s^2 2s^2\ ^1S)$ at 400 eV.

4 Results and discussion

Before presenting the calculated cross-section results, let us briefly discuss the experimental results previously published [1,2]. Figure 4 shows a map of the differential cross-section at $E_0 = 400$ eV resolved both in the angle θ_L and energy gain/loss $\Delta(E)$ variables. The parabolic border along which the cross-section peaks are located is given by equation (4) with $Q \sim 33.4$ eV, which corresponds to the transition from C^{4+} ground-state to C^{2+} ground state. In the following, we compare theoretical data to the measurements by Hoshino et al. published previously [1,2].

The angle differential cross-sections calculated for $E_0 = 270$, 400 and 470 eV are shown in Figures 5, 6 and 7 (full lines), along with the experimental data. It can be seen that the previous experiments could not resolve well oscillatory structures in the θ_L dimension. In Figures 5 and 7, a better agreement could be obtained if the experimental data are shifted by 1 deg and 0.5 deg,

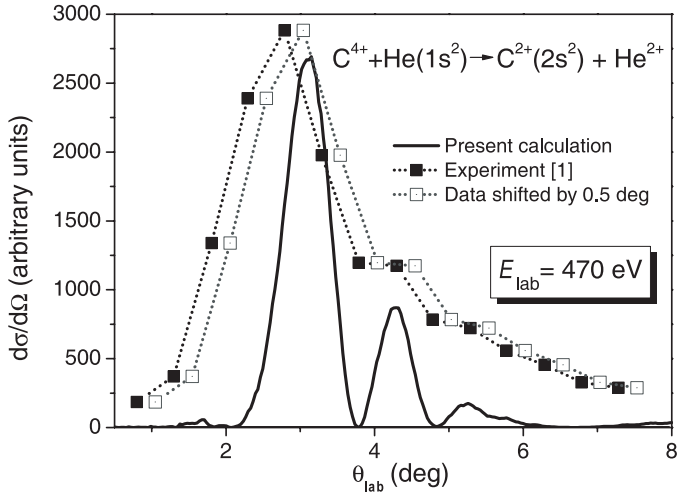

Fig. 7. Angle-differential cross-section for electron double capture to $C^{2+}(1s^2 2s^2\ ^1S)$ at 470 eV.

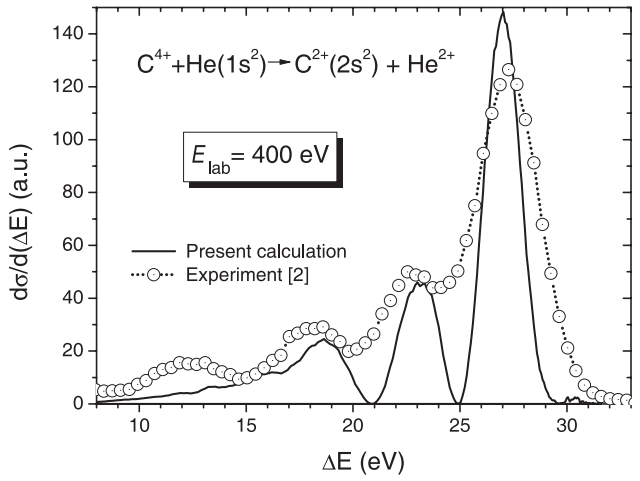

Fig. 8. Energy-gain differential cross-section for double electron capture to $C^{2+}(1s^2 2s^2\ ^1S)$ at 400 eV.

respectively. Such a shift is still consistent with the experimental error bars reported in [1,2]. Our results indicate that such a systematic correction of the experimental data could be appropriate, although the angular resolution of previous experiment is somewhat low. Next, the situation substantially improves when we compare with the differential cross-sections resolved in the energy gain/loss variable ΔE, i.e. the two-dimensional map in Figure 4 integrated over the θ_{lab} variable. Since the experimental cross-sections are subject to much smaller errors in $\Delta(E)$, the oscillatory cross-section structures in Figure 8 are now much better resolved. The agreement of the present results with experiment in Figure 8 is considered to be very good, especially when taking into account the sensitivity of differential cross-sections to the details of ab initio potentials and couplings. Since the energy resolution in the experiment is about 1 eV (250 meV/q for scattering ion analyzer), the full depth of the cross-section minima could not be resolved in the measurements.

The calculated angle-differential cross-sections in Figures 5–7 clearly show the existence of Stueckelberg oscillations. Due to relatively weak coupling of other channels, the cross-section minima fall near zero, which is a typical feature for two-state systems. Therefore in order to assess the applicability of two-state classical models to the present results, we have also calculated the semiclassical phases on the ab-initio adiabatic potentials, i.e.

$$\theta_{CMS,i}(b) = \pi - 2b \int_{R_{t,i}}^{R_x} \frac{\mathrm{d}R}{R^2(1 - U_i(R)/E - b^2/R^2)^{1/2}}, \tag{7}$$

$i = 1, 2$. Here $R_{t,i}$ is the turning point on adiabatic potential U_i and R_x the crossing point. The Stueckelberg phase in the semiclassical model is then given by the phase integral of the inverse function along the two $b_i(\theta)$ branches [3],

$$\phi(\theta_{CMS}) = \sqrt{2mE} \int_{\theta(R_x)}^{\theta_{CMS}} (b_1(\theta) - b_2(\theta))\mathrm{d}\theta. \tag{8}$$

The oscillatory factor $\cos(\phi(\theta_{lab}))$ shown in Figure 6 as a dashed line differs considerably from the rigorous result. Neither the frequency of oscillations nor their location is correctly reproduced. We attribute the reasons for which the semiclassical formalism does not apply well in this case especially to (1) the delocalized character of nonadiabatic transition at the crossing point, and (2) a neglect of transition phases at the crossing point.

5 Concluding remarks

We have calculated the differential cross-sections for double electron capture to C^{2+} ground-state in the collisions of C^{4+} with He based on ab initio potentials and couplings. The double electron capture channel to $C^{2+}(1s^2 2s^2\ ^1S)$ by far dominates capture to other states, which could be explained by the analysis of the crossing point in the delocalized transition region. The present diabatic potential matrices and double capture cross-sections differ from those based on the 2-state model [3]. The Stueckelberg oscillations in the calculated results could not be resolved in the data measured by Hoshino et al. [1,2] because of insufficient resolution in the experiment. On the other hand, the oscillatory structures in the energy gain differential cross-sections agree very well with the experimental data, suggesting this kind of spectroscopy to be a useful tool for studying state-resolved electron capture processes. Further experimental work is in progress to confirm the cross-section structures seen in the theoretical calculation.

This work was supported in part by the Japan Society for the Promotion of Science (JSPS), the Japanese Ministry of Science, Sports, Culture and Education (MEXT), and by the grant BU 450/7-3 of the Deutsche Forschungsgemeinschaft and the Fonds der Chemischen Industrie. L. Pichl acknowledges support by a JSPS Grant-in-Aid, Max Planck Society, and the Academic Frontier Program by MEXT. Special thanks are due to Prof. T. Kasai.

References

1. M. Hoshino, M. Kitajima, Y. Kanai, Y. Nakai, H. Tanaka, Y. Yamazaki, Phys. Scripta T **92**, 339 (2001)
2. M. Hoshino, Y. Kanai, F. Mallet, Y. Nakai, M. Kitajima, H. Tanaka, Y. Yamazaki, Nucl. Instrum. Meth. Phys. Res. B **205**, 568 (2003)
3. H. Danared, A. Barany, J. Phys. B: At. Mol. Phys. **19**, 3109 (1986)
4. M. Barat, P. Roncin, L. Guillemot, M.N. Gaboriaud, H. Laurent, J. Phys. B: At. Mol. Phys. **23**, 2811 (1990)
5. N. Keller, L.R. Andersson, R.D. Miller, M. Westerlind, S.B. Elston, I.A. Sellin, C. Biedermann, H. Cederquist, Phys. Rev. A **48**, 3684 (1993)
6. M. Kimura, R.E. Olson, J. Phys. B: At. Mol. Phys. **17**, L713 (1984)
7. T.P. Grozdanov, R.K. Janev, J. Phys. B: At. Mol. Phys. **13**, 3431 (1980)
8. R. Bloyd, T.-S. Ho, H. Rabitz, J. Chem. Phys. **106**, 6548 (1997)
9. R.J. Buenker, S.D. Peyerimhoff, Theo. Chim. Acta **35**, 33 (1974); R.J. Buenker, S.D. Peyerimhoff, Theo. Chim. Acta. **39**, 217 (1975); R.J. Buenker, Int. J. Quant. Chem. **29**, 435 (1986); S. Krebs, R.J. Buenker, J. Chem. Phys. **103**, 5613 (1995)
10. T.H. Dunning Jr, J. Chem. Phys. **90**, 1007 (1989)
11. E.E. Nikitin, S.Ya. Umanskii, *Theory of Slow Atomic Collisions* (Springer, New York, 1984)
12. T.G. Heil, S.E. Butler, A. Dalgarno, Phys. Rev. A **23**, 1100 (1981)
13. L.B. Zhao, P.C. Stancil, H.P. Liebermann, P. Funke, R.J. Buenker, Phys. Rev. A **71**, 060701:1 (2005)
14. T.G. Heil, J.B. Sharma, Phys. Rev. A **36**, 3669 (1987)
15. W. Fritsch, C.D. Lin, Phys. Rev. A **54**, 4931 (1996)
16. M. Kimura, N.F. Lane, Adv. At. Mol. Opt. Phys. **26**, 79 (1989)